CrystEngComm

PAPER

View Article Online
View Journal | View Issue

Cite this: *CrystEngComm*, 2015, **17**, 6591

Solvent modulated assembly of two Zn metal–organic frameworks: syntheses, luminescence, and gas adsorption properties†

Liangliang Zhang,*[a] Yu Zhang,[a] Rongming Wang,[a] Zixi Kang,[a] Xiaobin Liu,[a] Daofeng Sun[a] and Qingguo Meng*[b]

Received 29th April 2015,
Accepted 23rd July 2015

DOI: 10.1039/c5ce00833f

www.rsc.org/crystengcomm

A 2D wave-like layered framework based on benzotriazole-5-carboxylic acid (H_2btca), 2,2′-bipy and zinc ions – $[Zn(btca)(2,2'\text{-bipy})]_n$ (**1**) – has been resoundingly designed and synthesized by a solvothermal method. By changing the solvent from DMF to DMA, a 3D porous framework – $[Zn_2(btca)_2(bpy)(H_2O)]_n{\cdot}n$(DMA) (**2**) – was obtained. Complexes **1** and **2** have been determined by single-crystal X-ray diffraction analysis and further characterized by powder X-ray diffraction (PXRD), elemental analysis, IR spectroscopy, and thermogravimetric (TG) analysis. Complex **1** shows an AA packing 2D layered structure and complex **2** displays a 3D open honeycomb framework with a (3,4)-connected 2-nodal **fsc** topology. Moreover, gas adsorption of **2a** (the activated form of **2**) and the luminescence properties of **1**, **2** and **2a** have also been investigated intensively.

Introduction

Rational design and assembly of porous metal–organic frameworks (MOFs) have attracted much interest in the past few decades due to their versatile intriguing architectures and potential applications as multi-functional materials, such as in gas adsorption and separation, sensing, catalysis, and drug delivery.[1] Many functional MOFs of transition metal ions with interesting architectures and topologies have been well-established and synthesized successfully.[2] A number of factors might affect the structures and properties of MOF materials such as the choice of organic ligand, variety of metal centers, solvents, the pH value of the solution, the temperature, the counter ions, the template and metal-to-ligand stoichiometry, *etc.*[3] As we all know, organic ligands play a key role in self-assembly and in determining the structural and functional properties of porous MOFs.[4]

Benzotriazole-5-carboxylic acid (H_2btca) is a good bridging ligand for constructing multi-dimensional polymers and has multiple coordination sites,[5] which involves three benzotriazole nitrogen atoms and two carboxylate oxygen atoms. The resonance structures of the multi-dentate rigid $Hbtca^-$ ligand are shown in Scheme 1. Considering the structure of H_2btca, the introduction of nitrogen donor groups into the organic ligand will enhance the energetics and the resultant gas adsorption amount in MOF materials, such as CO_2.[6] Furthermore, H_2btca bearing a triazole functionality may improve the value of Q_{st} (~5 kJ mol^{-1}), which was exemplified by MTAF-3.[7] Moreover, derivatives of benzotriazole are important ultraviolet absorbing compounds in industry. However, to the best of our knowledge, 3D porous MOFs based on the H_2btca ligand are rarely reported. Li's group reported a porous MOF, namely $[Zn_3(OH)_2(btca)_2]{\cdot}DMF{\cdot}4H_2O$ with both significant breathing effect and photoluminescent response, during the gradual guest removal processes.[8] Chen's group reported 3D homometallic MOFs, whose magnetic transitions could be induced by desolvation.[9] Huang *et al.* presented a 3D framework with 1D honeycomb channels constructed by strip-shaped chains containing $[Cu_5(\mu_3\text{-}OH)_2(btca)_4]^-$ pentaclusters bridging to the adjacent $Cu_6(btca)_{12}^{6-}$ cages.[10] Han and Zeng described Mn-based homometallic MOFs, which display high H_2 adsorption ability at a lower pressure.[11]

Meanwhile, the solvent is another very significant factor in modulating the framework topology and the dimensionality

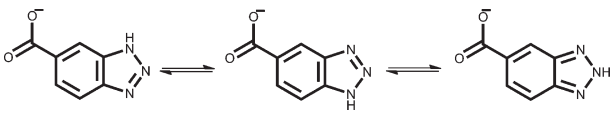

Scheme 1 Resonance structures of the $Hbtca^-$ ligand.

[a] *State Key Laboratory of Heavy Oil Processing, China University of Petroleum (East China), College of Science, China University of Petroleum (East China), Qingdao, Shandong 266580, People's Republic of China.*
E-mail: liangliangzhang@upc.edu.cn
[b] *Chemistry & Chemical and Environmental Engineering College, Weifang University, Weifang 261061, People's Republic of China*

† Electronic supplementary information (ESI) available: Selected bond lengths (Å) and angles (°) for complexes **1** and **2**, PXRD patterns, TGA curves, IR spectra, photophysical data, and excitation spectra. For ESI and crystallographic data in CIF or other electronic format see DOI: 10.1039/c5ce00833f

by acting as a coordination ligand or as a template for the assembly.[12] To some extent the kinetic and/or thermodynamic conformers could be controlled by changing the solvent. The coordination mode and the configuration of the ligand may be affected seriously by the solvent, particularly for the flexible carboxylic and imidazole ligands.[13]

Herein, we report two new MOFs $[Zn(btca)(bpy)]_n$ (**1**) and $[Zn_2(btca)_2(bpy)(H_2O)]_n{\cdot}n(DMA)$ (**2**) modulated solely by different solvents based on the H_2btca ligand and the Zn ions. The luminescence properties and gas adsorption of **2a** have also been investigated intensively.

Experimental section

Materials and methods

All chemical reagents were used as commercially obtained without further purification. The IR spectra were recorded on a Nicolet 330 FTIR spectrometer in the range of 4000–400 cm^{-1}. The thermogravimetric experiments (TGA) were performed using a Mettler-Toledo thermogravimetric analyzer. The powder X-ray diffraction experiments were measured using a Bruker AXS D8 Advance instrument diffractometer working with Cu Kα radiation, and the recording speed was 5° min^{-1} over the 2θ range of 5–50° at room temperature. The photoluminescence spectra were recorded using a Hitachi F-7000 fluorescence spectrophotometer. Elemental analyses (C, H and N) were carried out on a Perkin-Elmer 240 elemental analyzer. Gas sorption measurements were conducted using a Micromeritics ASAP 2020 system by using various gases and temperatures. The fluorescence lifetimes were measured on a FLS920 using a time correlated single photon counting (TCSPC) method by excitation with a 375 nm picosecond laser (EPL 445). The data were deconvoluted with the instrument response function, recorded with dispersed light, and fitted to a multi-exponential function. The absolute fluorescence quantum yields were measured with an integrating sphere.

Synthesis of complex 1

H_2btca (5 mg, 0.03 mmol), 2,2′-bipy (9 mg, 0.05 mmol) and $Zn(NO_3)_2{\cdot}4H_2O$ (22 mg, 0.07 mmol) were dissolved in a 1 mL mixture of *N*,*N*′-dimethylformamide (DMF) and H_2O (v/v = 1 : 1). The clear solution was sealed in a glass tube and placed into a programmed oven, slowly heated to 140 °C from room temperature in 500 minutes, kept at 140 °C for 5300 minutes, then slowly cooled to 30 °C in 800 minutes. A large amount of colorless block crystals of **1** were separated in 84% yield based on H_2btca. Elemental analysis calcd (%) for **1**: $C_{17}H_{11}N_5O_2Zn$: C, 53.36; H, 2.90; N, 18.30. Found: C, 52.75; H, 2.73; N, 17.99. IR data (KBr cm^{-1}): 1662(w), 1587(s), 1551(s), 1470(w), 1407(s), 1158(w), 1019(w), 771(m), 709(w).

Synthesis of complex 2

H_2btca (5 mg, 0.03 mmol), 2,2′-bipy (9 mg, 0.05 mmol) and $Zn(NO_3)_2{\cdot}4H_2O$ (22 mg, 0.07 mmol) were dissolved in a 1 mL mixture of *N*,*N*′-dimethylacetamide (DMA) and H_2O (v/v = 1 : 1). The clear solution was sealed in a glass tube and placed into a programmed oven, slowly heated to 140 °C from room temperature in 500 minutes, kept at 140 °C for 5300 minutes, then slowly cooled to 30 °C in 800 minutes. A large amount of colorless block crystals of **2** were separated in 70% yield based on H_2btca. Elemental analysis calcd (%) for **2**: $C_{28}H_{25}N_9O_6Zn_2$: C, 47.08; H, 3.53; N, 17.65. Found: C, 47.75; H, 4.01; N, 16.99. IR data (KBr cm^{-1}): 3440(s), 1640(s), 1602(m), 1564(w), 1404(m), 1280(w), 794(w), 755(w), 599(w), 455(w).

Single-crystal X-ray structural analysis

The single crystal data were collected on a SuperNova diffractometer equipped with a molybdenum micro-focus X-ray source (λ = 0.71073 Å) and an Eos CCD detector under 293 K. The data were collected with a ω-scan technique and an arbitrary φ-angle. Data reduction was performed with the CrysAlisPro package,[14] and an analytical adsorption correction was performed. The structures were solved by direct methods and refined by full-matrix least-squares on F^2 with anisotropic displacement using the SHELXTL software package.[15] The non-H atoms were treated anisotropically, whereas the aromatic and hydroxy hydrogen atoms were placed in calculated, ideal positions and refined as riding on their respective carbon or oxygen atoms. The structures were examined using the Addsym subroutine of PLATON[16] to assure that no additional symmetry could be applied to the models. The crystallographic data has been deposited with the Cambridge Crystallographic Data Center, CCDC 1062110 for **1** and 1062111 for **2**. These data can be obtained from the Cambridge Crystallographic Data Center, 12, Union Road, Cambridge CB21EZ, U.K. Crystallographic data for **1**–**2** are summarized in Table 1.

Results and discussion

Structure of complex 1

The crystals of **1** were obtained under solvothemal conditions by mixing H_2btca, 2,2′-bipy and $Zn(NO_3)_2{\cdot}4H_2O$ in a mixture of DMF/H_2O (1 : 1) at 140 °C for 3 days. Crystallographic studies revealed that compound **1** exhibits a 2D wave-like layered framework and crystallizes in an orthorhombic system with space group *Pbca*. The asymmetric unit contains one Zn^{2+} ion, one $btca^{2-}$ ligand and one coordinated 2,2′-bipy ligand. As shown in Fig. 1a, the Zn^{2+} center adopts a six-coordinated distorted ZnN_4O_2 octahedral environment, in which N1 and N2 come from 2,2′-bipy ligand, N3 and N5 come from two different $btca^{2-}$ ligands, and the remaining coordinated sites are occupied by two oxygen atoms from one $btca^{2-}$ ligand. The average Zn–N and Zn–O distances range from 2.14366(45) and 2.2446(64) Å. The $btca^{2-}$ ligand in **1** adopts a tri-dentate coordination mode (Fig. 1b) to link three Zn centres *via* its two triazole nitrogen atoms (N3 and N5) and two oxygen atoms (O1 and O2), which results in the 2D wave-like layer of complex **1**. Classical hydrogen bonds were not found in complex **1**. Finally, the 2D layers are in contact to form a

Table 1 Crystallographic data for complexes **1** and **2**

	1	2
Empirical formula	$C_{17}H_{11}N_5O_2Zn$	$C_{28}H_{25}N_9O_6Zn_2$
Formula weight	382.68	714.31
Temperature (K)	293(2)	293(2)
Crystal system	Orthorhombic	Orthorhombic
Space group	*Pbca*	*Pbca*
a (Å)	17.4695(3)	18.580(4)
b (Å)	8.64315(13)	9.962(2)
c (Å)	19.7657(4)	32.732(8)
α (deg)	90.00	90.00
β (deg)	90.00	90.00
γ (deg)	90.00	90.00
Volume (Å^3)	2984.44(8)	6058(2)
Z	8	8
ρ_{calc} (g cm^{-3})	1.703	1.566
μ (mm^{-1})	2.493	1.641
F (000)	1552.0	2912.0
Data/restraints/parameters	2656/0/226	6995/30/410
Goodness-of-fit on F^2	1.053	1.114
Final *R* indices $[I > 2\sigma(I)]^a$	R_1 = 0.0237, wR_2 = 0.0638	R_1 = 0.0342 wR_2 = 0.0853
Final *R* indexes [all data]^a	R_1 = 0.0260, wR_2 = 0.0653	R_1 = 0.0408 wR_2 = 0.0881

^{a} $R_1 = \sum||F_o| - |F_c||/\sum|F_o|$. $wR_2 = [\sum w(F_o^2 - F_c^2)^2/\sum w(F_o^2)^2]^{0.5}$.

3D supramolecular framework in an AA stack fashion because of C–H···π and weak intramolecular hydrogen bond interactions (Fig. 1c). Complex **1** features C–H···O intermolecular hydrogen bonding interactions between C8 as the hydrogen atom donor and O1 (C8–H8···O1, H8 to O1 distance of 2.58 Å, C8–H8···O1 angle of 116°). Complex **1** also features intramolecular C–H···N hydrogen bonding interactions between C17 as the hydrogen atom donor and N4 (C17–H17···N4, H17 to N4 distance of 2.38 Å, C17–H17···N4 angle of 167(3)°) [symmetry code: (a) −0.5 + *x*, *y*, 0.5 − *z*; (b) 1 − *x*, −0.5 + *y*, 0.5 − *z*; (c) 0.5 + *x*, *y*, 0.5 − *z*; (d) 1 − *x*, 0.5 + *y*, 0.5 − *z*].

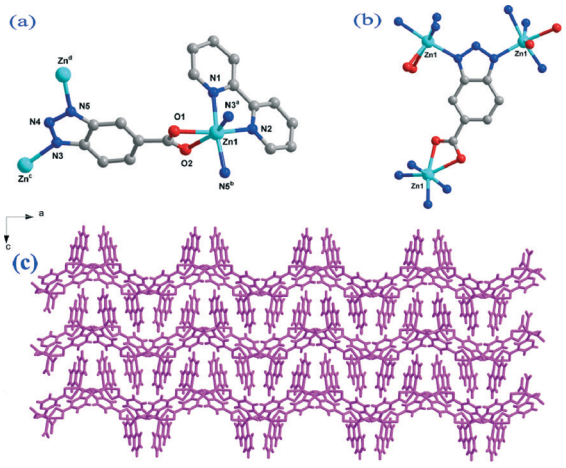

Fig. 1 (a) The coordination environment of the Zn(II) atoms in complex **1** (the hydrogen atoms are omitted for clarity). (b) The coordination mode of the H_2btca ligand. (c) The AA packing mode structure of **1** viewed along the *b* axis.

Structure of complex 2

Crystals of **2** were obtained under solvothemal conditions by mixing H_2btca, 2,2′-bipy and $Zn(NO_3)_2{\cdot}4H_2O$ in a mixture of DMA/H_2O (1 : 1) at 140 °C for 3 days. Crystallographic studies revealed that compound **2** crystallizes in an orthorhombic system with space group *Pbca*, and its asymmetric unit contains two Zn^{2+} ions, two btca$^-$ ligands, one 2,2′-bipyridine, and one lattice DMA molecule (Fig. 2a). Zn1 is four-coordinated with one oxygen and three nitrogen atoms from four different btca^{2-} ligands forming a tetrahedral geometry. The Zn2 ion in **2** adopts a distorted trigonal bipyramidal geometry. Each Zn2 ion is five-coordinated with one carboxylate oxygen atom from one btca^{2-} molecule, one oxygen atom from a coordinated water molecule, one nitrogen atom from one btca^{2-} molecule and two nitrogen atoms from one chelating 2,2′-bipy ligand. All the btca^{2-} ligands are in μ3 bridging mode through two btca^{2-} nitrogen atoms and a μ2:η1:η0 carboxylate group (Fig. 2b). One btca^{2-} ligand links three four-coordinated Zn1 centers and the other btca^{2-} ligand connects two five-coordinated Zn2 and one four-coordinated Zn1 centres, which give rise to the final 3D porous framework. The DMA molecules are located in the pore of complex **2** by hydrogen bonds between O1W from coordinated water and

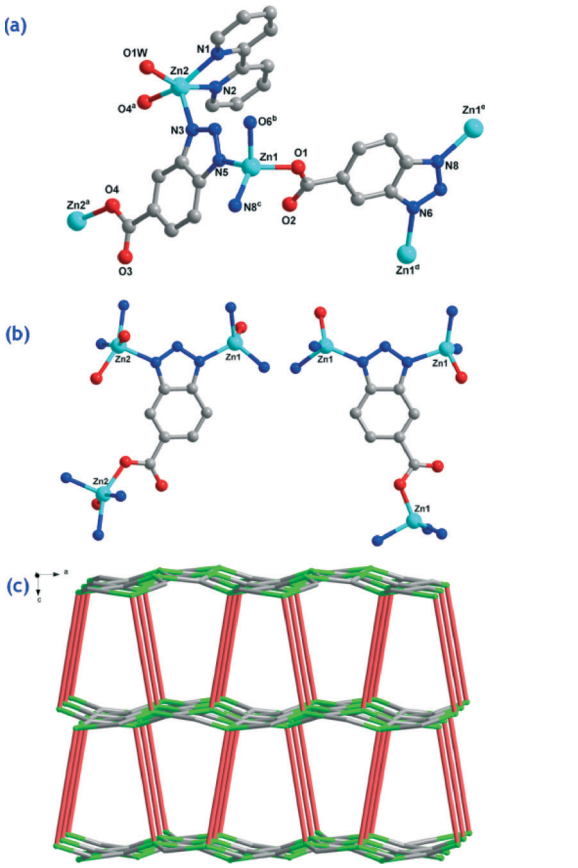

Fig. 2 (a) The coordination environment of the Zn(II) atoms in complex **2** (the hydrogen atoms are omitted for clarity). (b) The coordination mode of the H_2btca ligand. (c) The 3D net structure of **2** along the *b* axis.

O5 from DMA (O1Wa–H1Wa···O5, H1Wa to O5 distance of 1.83 Å, O1Wa–H1Wa···O5 angle of 157°) [symmetry code: (a) $-x, -y, -z$; (b) $0.5 - x, 0.5 + y, z$; (c) $-0.5 + x, y, 0.5 - z$; (d) $0.5 - x, -0.5 + y, z$; (e) $0.5 + x, y, 0.5 - z$].

From the topological point of view, the Zn1 atoms can be defined as 4-connected nodes, the organic ligands can be regarded as 3-connected nodes, and the $[(Zn_2)_2(btca)_2]$ dimer unit can be simplified as linkers (Fig. 2c). Thus, the overall structure of **2** can be described as a 3D 2-nodal (3,4)-connected **fsc** framework with a Schläfli symbol of $\{6^3\cdot8^3\}\{6^3\}$ calculated with TOPOS.[17] The potential free volume of **2** is 65.1% as calculated by PLATON (1.8 Å probe radius) after removal of the guest solvent molecules (Fig. 3).

Powder X-ray diffraction (PXRD) measurements were performed to confirm phase purity. The experimental PXRD is consistent with the PXRD pattern calculated based on the crystal structure using Mercury 3.3 (Fig. S1 and S2, ESI†). Thermogravimetric analysis (TGA) experiments performed on the as-synthesized **1**, **2** and **2a** reveal moderate thermal stabilities (Fig. S3, ESI†).

Gas adsorption measurements

The permanent porosity of complex **2a** prompted us to investigate the gas adsorption ability. The measurement of the adsorption properties of complex **2a** was performed on a Micromeritics ASAP 2020 system. Complex **2** was sequentially exchanged with methanol and dichloromethane for three days, and the degassing process was performed at 60 °C for 5 hours. The gas sorption capabilities of complex **2a** were investigated using several gases (N_2, H_2, CH_4, Ar and CO_2) at varying temperatures.

The permanent porosity of the activated sample **2a** was confirmed by the N_2 sorption experiment at 77 K. As shown in Fig. 4, the fully activated sample reveals a typical type-I behavior as expected for microporous materials, and the pore size is 1.48 nm, which is coincidental with the crystal structure. The adsorption isotherms of N_2 have an abrupt slope from 0.01 to 0.1 bar, which reveals that the pores are filled as the pressure is increased from 0.01 to 0.1 bar. Then the uptake capacity of N_2 increases slightly and reaches a platform at 98 cm^3g^{-1} at 1 bar. Derived from N_2 adsorption, the Langmuir surface area of **2a** is 426 $m^2\ g^{-1}$, the Brunauer–Emmett–Teller (BET) surface area and total pore volume are 384 $m^2\ g^{-1}$ and 0.161 $cm^3\ g^{-1}$, respectively. The obtained pore volume is much smaller than that (0.638 $cm^3\ g^{-1}$) calculated from the X-ray data, which is due to the reduced volume of the activated phase of **2a** after the lattice solvents were eliminated. The desolvated **2a** also adsorbs Ar, and the maximum uptake amounts to 99.5 $cm^3\ g^{-1}$ at 1 atm and 77 K (Fig. S4, ESI†). The Brunauer–Emmett–Teller (BET) surface area, the Langmuir surface area and the total pore volume obtained from the Ar isotherm are 263 $m^2\ g^{-1}$, 329 $m^2\ g^{-1}$and 0.412 $cm^3\ g^{-1}$, respectively.

The H_2 and CH_4 adsorption isotherms of activated **2a** are also measured. As depicted in Fig. 5, the activated **2a** can adsorb 56.5 $cm^3\ g^{-1}$ (~0.5 wt%) of H_2 at 77 K and 1 bar and 14.5 $cm^3\ g^{-1}$ (~1.0 wt%) of CH_4 at 273 K and 1 bar. The maximum H_2 uptake of **2a** at low pressures is relatively lower than the high capacity coordination framework reported to date, such as Cu_2(BPTC)[18] and IRMOF-1,[19] which display high capacities of H_2 uptake (~2.47 wt% and 1.32 wt%) under similar conditions (77 K and 1 atm). The isosteric heat of H_2

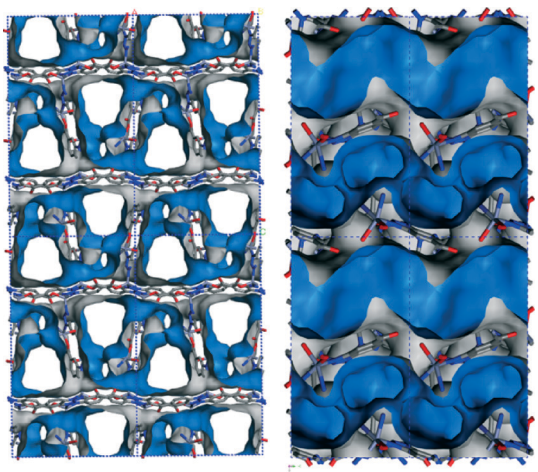

Fig. 3 (Left and right) Connolly surface representation along the *b* and *c* axes, respectively, showing that complex **2** is porous and comprises interconnected pores.

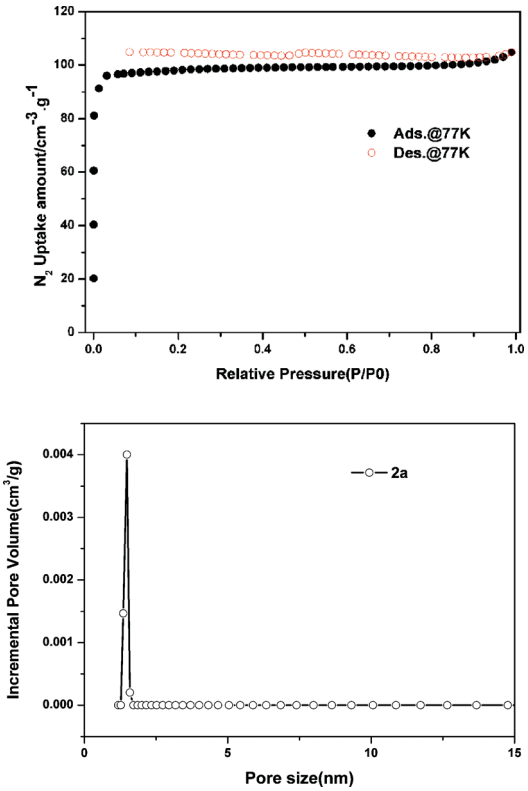

Fig. 4 The nitrogen adsorption isotherms (up) at 77 K and the corresponding pore size distribution curves (down) for **2a**.

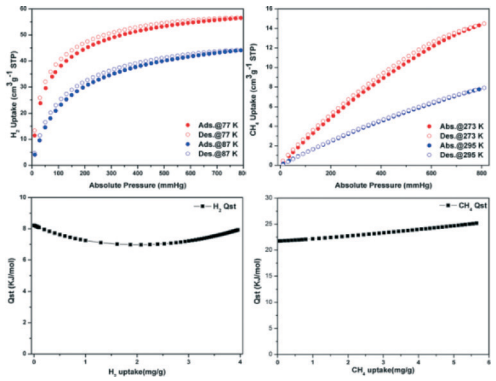

Fig. 5 The H_2 and CH_4 sorption isotherms for **2a** (left and right). H_2: red, 77 K; blue, 87 K. CH_4: red, 273 K; blue, 295 K. Isosteric heats of H_2 and CH_4 adsorption (Q_{st}) for complex **2a**.

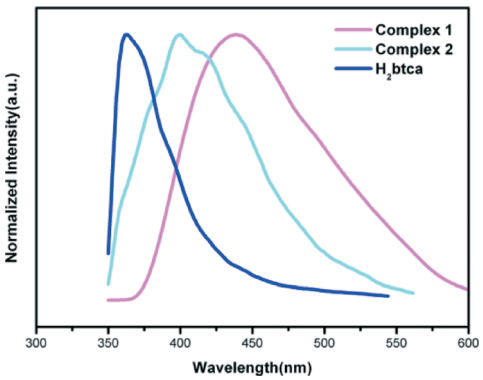

Fig. 6 The luminescence spectra of H_2btca, complexes **1** and **2**.

adsorption (Q_{st}) value of complex **2a**, determined by applying the Clausius–Clapeyron equation to the isotherms obtained at 77 and 87 K, is approximately 7.5 kJ·mol^{-1} at low coverage, which is higher than those of non-N-containing MOFs, such as the NOTT series (5.68–6.70 kJ mol^{-1}),[20a] $Cu_6(BTTC)_4(H_2O)_6 \cdot xS$, (7.0 kJ mol^{-1}),[20b] UMCM-150 (6.3 kJ mol^{-1}),[20c] MIL-100 (6.3 kJ mol^{-1})[20d] and MIL-102 (6.0 kJ mol^{-1}).[20e] The isosteric heat value of CH_4 is 21.6 kJ·mol^{-1}, which was obtained at 273 and 295 K. Interestingly, the CO_2 adsorption isotherms of activated **2a** are also investigated. The CO_2 adsorption isotherm at 273 K indicated a clear terrace in the range of 155–330 mmHg. After this pressure, the uptake volume suddenly increased. This indicates that the structure could be transformed into a new structure during this period of CO_2 adsorption and the maximum uptake of CO_2 is 40.0 cm^3 g^{-1}. The desorption isotherm also displayed a sharp step at 407 mmHg. When the measurement temperature was increased to 295 K, the adsorption isotherm did not show the characteristic step, and the uptake volume dramatically decreased to 21.95 cm^3 g^{-1} as shown in Fig. S5.† On the basis of the stepped CO_2 isotherms with a large hysteresis between the adsorption and the desorption branches at 273 K and significantly decreased adsorption amounts at higher temperatures, these results also imply that **2a** is a dynamic framework.[21]

Luminescence properties of complexes 1, 2 and 2a

The various interesting luminescence properties MOFs possess are ascribed to their application in chemical sensors, photochemistry, electroluminescence display, and so on.[22] Generally, d^{10} transition metal complexes are promising materials that can exhibit photoluminescence properties.[23] In addition, organic ligands, their coordination modes and different metals, evidently affect the emission wavelength and luminescence theory.[24] In this work, the solid-state photoluminescence spectra of btca^{2-}, complexes **1** and **2** have been measured at room temperature (Fig. 6). The H_2btca ligand displays photoluminescence with an emission maxima at 362 nm (λ_{ex} = 300 nm), which can be ascribed to the $\pi \rightarrow \pi^*$ transitions.[25] Upon complexation of H_2btca and 2,2′-bipy ligands with the Zn(II) ion, an intense emission is observed at 441 nm (λ_{ex} = 330 nm) for **1** and 400 nm (λ_{ex} = 295 nm) for **2**, respectively. Since the Zn(II) ions are difficult to oxidize or reduce due to their d^{10} configurations, emission of complexes **1** and **2** is neither metal-to-ligand charge transfer (MLCT) nor ligand-to-metal charge transfer (LMCT) in nature. Thus, emission of **1** and **2** is probably attributed to the intraligand $\pi \rightarrow \pi^*$ transitions modified by metal coordination. In comparison with H_2btca, a red shift of 38 nm has been observed in **1** and 79 nm in **2**, which are probably attributable to the different coordination modes of the H_2btca ligands. It may affect the rigidity of the solid-state crystal packing and further influence their luminescence emission bands. Furthermore, a time-resolved luminescence study was performed on the complexes **1**, **2** and **2a** by monitoring the most intense emission at ambient temperature. The decay curves can be fitted well as shown in Fig. 7, and the detailed data are listed in Table S3 in the ESI.† The τ values of complexes **1**, **2** and **2a** were fitted to a tri-exponential decay curve. The lifetime (τ) is defined as the time in which the fluorescence intensity decays to 1/e of the initial intensity (I_o), where e is the natural log constant and is equal to 2.718. The quantum yield (Φ) of complexes **1**, **2** and **2a** were 2.72%, 2.85% and 4.35%, respectively.

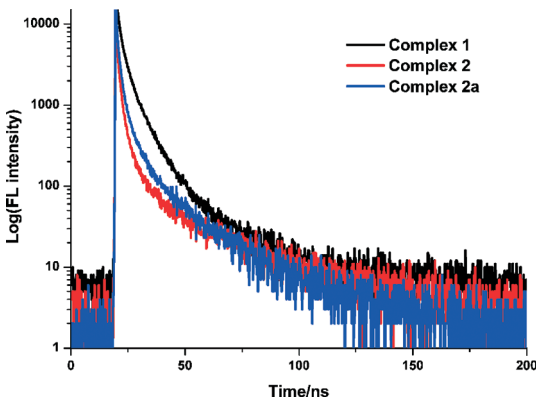

Fig. 7 The solid state luminescence decay curves of complexes **1**, **2** and **2a**.

Conclusions

In summary, two new MOFs based on H_2btca and zinc – $[Zn(btca)(2,2'\text{-bipy})]_n$ (**1**) and $[Zn_2(btca)_2(bpy)(H_2O)]_n \cdot n(DMA)$ (**2**) – have been designed and synthesized by modulating the solvent. Complex **1** displays a 2D layered structure and complex **2** shows a (3,4)-connected 2-nodal **fsc** topology. Gas sorption for **2a** gives a Langmuir surface area of 426 $m^2\ g^{-1}$, 56.5 $cm^3\ g^{-1}$ (~0.5 wt%) of H_2 at 77 K and 1 bar and 14.5 $cm^3\ g^{-1}$ (~1.0 wt%) of CH_4 at 273 K and 1 bar. In addition, the solid-state photoluminescence spectra of **1** and **2** exhibit a red shift of 38 and 79 nm, respectively, compared to the H_2btca ligand.

Acknowledgements

We thank Dr. H. Y. Liu and Prof. X. Y. Li (UPC) for assistance with the fluorescence lifetime and quantum yield of the MOF samples. This work was supported by the NSFC (grant no. 21271117), the Shandong Provincial Natural Science Foundation (ZR2015BM005), and the Fundamental Research Funds for the Central Universities (13CX05010A, 14CX02158A, 14CX02150A), a Project of Shandong Province Higher Educational Science and Technology Program (J14LA52).

Notes and references

1 (*a*) H. Furukawa, K. E. Cordova, M. O'Keeffe and O. M. Yaghi, *Science*, 2013, **341**, 974; (*b*) M. O'Keeffe and O. M. Yaghi, *Chem. Rev.*, 2012, **112**, 675; (*c*) J. P. Zhang, Y. B. Zhang, J. B. Lin and X. M. Chen, *Chem. Rev.*, 2012, **112**, 1001; (*d*) X. C. Shan, F. L. Jiang, D. Q. Yuan, H. B. Zhang, M. Y. Wu, L. Chen, J. Wei, S. Q. Zhang, J. Pan and M. C. Hong, *Chem. Sci.*, 2013, **4**, 1484; (*e*) Y. W. Li, K. H. He and X. H. Bu, *J. Mater. Chem. A*, 2013, **1**, 4186; (*f*) J. R. Li, J. Sculley and H. C. Zhou, *Chem. Rev.*, 2011, **112**, 869; (*g*) Y. P. Li, H. R. Yang, Q. Zhao, W. C. Song, J. Han and X. H. Bu, *Inorg. Chem.*, 2012, **51**, 9642.

2 (*a*) J. R. Long and O. M. Yaghi, *Chem. Soc. Rev.*, 2009, **38**, 1213; (*b*) J. L. C. Rowsell, E. C. Spencer, J. Eckert, J. A. K. Howard and O. M. Yaghi, *Science*, 2005, **309**, 1350; (*c*) T. R. Cook, Y. R. Zheng and P. J. Stang, *Chem. Rev.*, 2013, **113**, 734; (*d*) W. Zhang and R. G. Xiong, *Chem. Rev.*, 2012, **112**, 1163; (*e*) P. S. Nugent, V. L. Rhodus, T. Pham, K. Forrest, L. Wojtas, B. Space and M. J. Zaworotko, *J. Am. Chem. Soc.*, 2013, **135**, 10950; (*f*) H. L. Sun, Z. M. Wang and S. Gao, *Coord. Chem. Rev.*, 2010, **254**, 1081.

3 (*a*) J. Ma, L. Chen, M. Y. Wu, S. Q. Zhang, K. C. Xiong, D. Han, F. L. Jiang and M. C. Hong, *CrystEngComm*, 2013, **15**, 911; (*b*) M. Du, C. P. Li, C. S. Liu and S. M. Fang, *Coord. Chem. Rev.*, 2013, **257**, 1282; (*c*) Y. L. Gai, F. L. Jiang, K. C. Xiong, L. Chen, D. Q. Yuan, L. J. Zhang, K. Zhou and M. C. Hong, *Cryst. Growth Des.*, 2012, **12**, 2079; (*d*) L. N. Li, S. Y. Wang, T. L. Chen, Z. H. Sun, J. H. Luo and M. C. Hong, *Cryst. Growth Des.*, 2012, **12**, 4109.

4 (*a*) X. J. Li, F. L. Jiang, M. Y. Wu, S. Q. Zhang, Y. F. Zhou and M. C. Hong, *Inorg. Chem.*, 2012, **51**, 4116; (*b*) Y. Q. Chen, S. J. Liu, Y. W. Li, G. R. Li, K. H. He, Z. Chang and X. H. Bu, *CrystEngComm*, 2013, **15**, 1613; (*c*) S. Bureekaew, H. Sato, R. Matsuda, Y. Kubota, R. Hirose, J. Kim, K. Kato, M. Takata and S. Kitagawa, *Angew. Chem., Int. Ed.*, 2010, **49**, 7660.

5 Z. H. Li, L. P. Xue, B. T. Zhao, J. Kan and W. P. Su, *CrystEngComm*, 2012, **14**, 8485.

6 (*a*) Y. Liu, Z. U. Wang and H. C. Zhou, *Greenhouse Gases: Sci. Technol.*, 2012, **2**, 239; (*b*) R. Sabouni, H. Kazemian and S. Rohani, *Environ. Sci. Pollut. Res.*, 2013, **1**.

7 (*a*) W. Y. Gao, W. Yan, R. Cai, K. Williams, A. Salas, L. Wojtas, X. Shi and S. Ma, *Chem. Commun.*, 2012, **48**, 8898; (*b*) R. Luebke, L. J. Weselinski, Y. Belmabkhout, Z. J. Chen, L. Wojtas and M. Eddaoudi, *Cryst. Growth Des.*, 2014, **14**, 414.

8 J. Xiao, Y. Wu, M. Li, B. Y. Liu, X. C. Huang and D. Li, *Chem. – Eur. J.*, 2013, **19**, 1891.

9 X. M. Zhang, Z. M. Hao, W. X. Zhang and X. M. Chen, *Angew. Chem.*, 2007, **119**, 3526.

10 J. Xiao, B. Y. Liu, G. Wei and X. C. Huang, *Inorg. Chem.*, 2011, **50**, 11032.

11 Z. B. Han, R. Y. Lu, Y. F. Liang, Y. L. Zhou, Q. Chen and M. H. Zeng, *Inorg. Chem.*, 2012, **51**, 674.

12 (*a*) I. S. Lee, D. M. Shin and Y. K. Chung, *Chem. – Eur. J.*, 2004, **10**, 3158; (*b*) P. Pachfule, R. Das, P. Poddar and R. Banerjee, *Cryst. Growth Des.*, 2011, **11**, 1215.

13 (*a*) H. Y. He, D. Collins, F. N. Dai, X. L. Zhao, G. Q. Zhang, H. Q. Ma and D. F. Sun, *Cryst. Growth Des.*, 2010, **10**, 895; (*b*) J. Guo, L. L. Zhang, H. Q. Ma, Z. Chen, D. Sun, Y. H. Wei and D. F. Sun, *Inorg. Chem. Commun.*, 2013, **28**, 75; (*c*) J. P. Zhang, X. C. Huang and X. M. Chen, *Chem. Soc. Rev.*, 2009, **38**, 2385.

14 *CrysAlisPro (Version 1.171.31.7.)*, Agilent Technologies.

15 G. M. Sheldrick, *SHELXS-97, Program for X-ray Crystal Structure Determination*, University of Gottingen, Germany, 1997.

16 A. L. Spek, *PLATON, A Multipurpose Crystallographic Tool*, Utrecht University, Utrecht, The Netherlands, 2002.

17 V. A. Blatov, *IUCr CompComm Newsletter*, 2006, vol. 7, pp. 4–38, http://www.topos.ssu.samara.ru.

18 (*a*) M. Latroche, S. Surblé, C. Serre, C. Mellot-Draznieks, P. L. Llewellyn, J. H. Lee, J. S. Chang, S. H. Jhung and G. Férey, *Angew. Chem., Int. Ed.*, 2006, **45**, 8227; (*b*) H. Furukawa, M. A. Millerb and O. M. Yaghi, *J. Mater. Chem.*, 2007, **17**, 3197.

19 J. L. C. Rowsell and O. M. Yaghi, *Microporous Mesoporous Mater.*, 2004, **73**, 3.

20 (*a*) X. Lin, I. Telepeni, A. J. Blake, A. Dailly, C. M. Brown, J. M. Simmons, M. Zoppi, G. S. Walker, K. M. Thomas, T. J. Mays, P. Hubberstey, N. R. Champness and M. Schröder, *J. Am. Chem. Soc.*, 2009, **131**, 2159; (*b*) Y. M. Huang, B. G. Zhang, J. G. Duan, W. L. Liu, X. F. Zheng, L. L. Wen, X. H. Ke and D. F. Li, *Cryst. Growth Des.*, 2014, **14**, 2866; (*c*) A. G. Wong-Foy, O. Lebel and A. J. Matzger, *J. Am. Chem. Soc.*, 2007, **129**, 15740; (*d*) M. Latroche, S. Suble, C. Serre, C. Mellot-Draznieks, P. L. Llewellyn, J.-H. Lee, J.-S. Chang, S. H. Jhung and G. Férey, *Angew. Chem., Int. Ed.*, 2006, **45**, 8227; (*e*) S. Surblé, F. Millange, C. Serre, T. Düren, M. Latroche, S.

Bourrelly, P. L. Llewellyn and G. Férey, *J. Am. Chem. Soc.*, 2006, **128**, 14889.

21 (*a*) I. H. Hwang, J. M. Bae, Y. K. Hwang, H. Y. Kim, C. Kim, S. Huh, S. J. Kim and Y. Kim, *Dalton Trans.*, 2013, **42**, 15645; (*b*) P. V. Dau and S. M. Cohen, *CrystEngComm*, 2013, **15**, 9304.

22 S. Ma, D. F. Sun, J. M. Simmons, C. D. Collier, D. Yuan and H. C. Zhou, *J. Am. Chem. Soc.*, 2007, **130**, 1012.

23 (*a*) J. Guo, J. F. Ma, J. J. Li, J. Yang and S. X. Xing, *Cryst. Growth Des.*, 2012, **12**, 6074; (*b*) J. Guo, J. F. Ma, B. Liu, W. Q. Kan and J. Yang, *Cryst. Growth Des.*, 2011, **11**, 3609; (*c*) J. S. Hu, Y. J. Shang, X. Q. Yao, L. Qin, Y. Z. Li, Z. J. Guo, H. G. Zheng and Z. L. Xue, *Cryst. Growth Des.*, 2010, **10**, 2676; (*d*) J. Yang, Q. Yuo, G. D. Li, J. J. Cao, G. H. Li and J. S. Chen, *Inorg. Chem.*, 2006, **45**, 2857.

24 (*a*) H. C. Fang, J. Q. Zhu, L. J. Zhou, H. Y. Jia, S. S. Li, X. Gong, S. B. Li, Y. P. Cai, P. K. Thallapally, J. Liu and G. J. Exarhos, *Cryst. Growth Des.*, 2010, **10**, 3277; (*b*) X. T. Rao, T. Song, J. K. Gao, Y. J. Cui, Y. Yang, C. D. Wu, B. L. Chen and G. D. Qian, *J. Am. Chem. Soc.*, 2013, **135**, 15559; (*c*) H. L. Jiang, D. W. Feng, K. C. Wang, Z. Y. Gu, Z. W. Wei, Y. P. Chen and H. C. Zhou, *J. Am. Chem. Soc.*, 2013, **135**, 13934; (*d*) S. Q. Zang, L. H. Cao, R. Liang, H. W. Hou and T. C. W. Mak, *Cryst. Growth Des.*, 2012, **12**, 1830; (*e*) X. Q. Liang, X. H. Zhou, C. Chen, H. P. Xiao, Y. Z. Li, J. L. Zuo and X. Z. You, *Cryst. Growth Des.*, 2009, **9**, 1041; (*f*) D. Niu, J. Yang, J. Guo, W. Q. Kan, S. Y. Song, P. Du and J. F. Ma, *Cryst. Growth Des.*, 2012, **12**, 2397.

25 E. Colacio, R. Kivekäs, F. Lloret, M. Sunberg, J. Suarez-Varela, M. Bardají and A. Laguna, *Inorg. Chem.*, 2002, **41**, 5141.